Available online at www.pelagiaresearchlibrary.com

Pelagia Research Library

Advances in Applied Science Research, 2012, 3 (6):3766-3787

Pelagia Research Library

ISSN: 0976-8610
CODEN (USA): AASRFC

Combined effects of Hall currents and radiation on MHD free convective Couette flow in a rotating system

Bhaskar Chandra Sarkar[1], Sanatan Das[2] and Rabindra Nath Jana[1]

[1]*Department of Applied Mathematics, Vidyasagar University, Midnapore 721 102, India*
[2]*Department of Mathematics, University of Gour Banga, Malda 732 103, India*

ABSRAECT

Effects of Hall currents and radiation on MHD free convection of a viscous incompressible fluid confined between two vertical walls in a rotating system have been studied. We have considered the flow due to the impulsive as well as accelerated motion of one of the walls. The governing equations are solved analytically using the Laplace transform technique. The variations of the fluid velocity components and the fluid temperature are presented graphically. It is found that the velocity components decrease near the moving wall and increase away from the moving wall for both the impulsive as well as the accelerated motion of one of the walls with an increase in Hall parameter. There is an enhancement in fluid temperature as time progresses. The absolute value of the shear stresses at the moving wall due to the primary and the secondary flows for both the impulsive as well as the accelerated motion increase with an increase in either rotation parameter or radiation parameter. The rate of heat transfer at the moving wall increases with an increase in radiation parameter.

Key words: MHD Couette flow, free convection, Hall currents, radiation, rotation, Prandtl number, impulsive motion and accelerated motion.

INTRODUCTION

Couette flow is one of the basic flow in fluid dynamics that refers to the laminar flow of a viscous fluid in the space between two parallel walls, one of which is moving and the other wall kepts at rest. The flow is driven by virtue of viscous drag force acting on the fluid. The radiative convective flows are frequently encountered in many scientific and environmental processes such as astrophysical flows, water evaporation from open reservoirs, heating and cooling of chambers and solar power technology. Heat transfer by simultaneous radiation and convection has applications in numerous technological problems including combustion, furnace design, nuclear reactor safety, fluidized bed heat exchanger, fire spreads, solar fans, solar collectors, natural convection in cavities, turbid water bodies, photo chemical reactors and many others. In an ionized gas where the density is low and/or the magnetic field is very strong, the conductivity normal to the magnetic field is reduced due to the free spiraling of electrons and ions about the magnetic lines of force before suffering collisions and a current is induced in a direction normal to both the electric and the magnetic fields. This current, well known in the literature, is called the Hall currents. Due to Hall currents the electrical conductivity of the fluid becomes anisotropic and this causes the secondary flow. Hall effects are important when the Hall parameter, which is the ratio between the electron-cyclotron frequency and the electron-atom-collision frequency, is high. This happens when the magnetic field is strong or when the collision frequency is low. Hall currents are of great importance in many astrophysical problems, Hall accelerator and flight

MHD as well as flows of plasma in a MHD power generator. The hydrodynamic rotating flow of an electrically conducting viscous incompressible fluid has gained considerable attention because of its numerous applications in physics and engineering. In geophysics, it is applied to measure and study the positions and velocities with respect to a fixed frame of reference on the surface of earth, which rotates with respect to an inertial frame in the presence of its magnetic field. The free convection in channels formed by vertical plates has received attention among the researchers in last few decades due to it's widespread importance in engineering applications like cooling of electronic equipments, design of passive solar systems for energy conversion, design of heat exchangers, human comfort in buildings, thermal regulation processes and many more. Many researchers have worked in this field viz. Singh [1], Singh et. al. [2], Jha et.al. [3], Joshi [4], Miyatake et. al. [5], Tanaka et. al. [6] and many others. Hall currents and surface temperature oscillations effects on natural convection magnetohydrodynamic heat-generating flow have been considered by Takhar and Ram [7]. The transient free convection flow between two vertical parallel plates has been investigated by Singh et al. [8]. Jha [9] has studied the natural Convection in unsteady MHD Couette flow. Thermal radiation effect on fully developed mixed convection flow in a vertical channel has been studied by Grosan and Pop [10]. Jha and Ajibade [11] have studied the unsteady free convective Couette flow of heat generating/absorbing fluid. Al-Amri et al. [12] have discussed the combined forced convection and surface radiation between two parallel plates. The effects of thermal radiation and free convection on the unsteady Couette flow between two vertical parallel plates with constant heat flux at one boundary have been studied by Narahari [13]. Rajput and Pradeep [14] have presented the effect of a uniform transverse magnetic field on the unsteady transient free convection flow of a viscous incompressible electrically conducting fluid between two infinite vertical parallel plates with constant temperature and variable mass diffusion. Rajput and Kumar [15] have discussed the combined effects of rotation and radiation on MHD flow past an impulsively started vertical plate with variable temperature. Reddy et al. [16] have presented the radiation and chemical reaction effects on free convection MHD flow through a porous medium bounded by vertical surface. The unsteady MHD heat and mass transfer free convection flow of polar fluids past a vertical moving porous plate in a porous medium with heat generation and thermal diffusion has been studied by Saxena and Dubey [17]. The mass transfer effects on MHD mixed convective flow from a vertical surface with Ohmic heating and viscous dissipation have been investigated by Babu and Reddy [18]. Saxena and Dubey [19] have analyzed the effects of MHD free convection heat and mass transfer flow of visco-elastic fluid embedded in a porous medium of variable permeability with radiation effect and heat source in slip flow regime. Devi and Gururaj [20] have studied the effects of variable viscosity and nonlinear radiation on MHD flow with heat transfer over a surface stretching with a power-law velocity. The radiation effect on the unsteady MHD convection flow through a non uniform horizontal channel has been studied by Reddy et al. [21]. Singh and Pathak [22] have studied the effect of rotation and Hall current on mixed convection MHD flow through a porous medium filled in a vertical channel in the presence of thermal radiation. Das et. al. [23] have investigated the radiation effects on free convection MHD Couette flow started exponentially with variable wall temperature in presence of heat generation. Effects of radiation on transient natural convection flow between two vertical walls have been discussed by Mandal et al.[24]. Recently, Sarkar et. al. [25-26] have studied the effects of radiation on MHD free convective Couette flow in a rotating system. Oscillatory MHD free convective flow between two vertical walls in a rotating system has been studied by Sarkar et. al. [27].

In the present paper, we have studied the effects of radiation on free convective MHD Couette flow of a viscous incompressible electrically conducting fluid in a rotating system in the presence of an applied transverse magnetic field on taking Hall currents into account. It is observed that the velocity components decrease near the moving wall and increase away from the moving wall for both the impulsive as well as the accelerated motion of one of the walls with an increase in Hall parameter m. The fluid temperature decreases with an increase in radiation parameter R whereas it increases with an increase in time τ. The absolute value of the shear stress τ_{x_0} due to the primary flow and the shear stress τ_{y_0} due to the secondary flow at the wall $(\eta = 0)$ for both the impulsive as well as the accelerated motion increase with an increase in either radiation parameter R or rotation parameter K^2. Further, the rate of heat transfer $-\theta'(0,\tau)$ at the wall $(\eta = 0)$ increases whereas the rate of heat transfer $-\theta'(1,\tau)$ at the wall $(\eta = 1)$ decreases with an increase in radiation parameter R.

FORMULATION OF THE PROBLEM AND ITS SOLUTION

Consider the unsteady free convection MHD Couette flow of a viscous incompressible electrically conducting fluid between two infinite vertical parallel walls separated by a distance h. Choose a Cartesian co-ordinates system with the x - axis along one of the walls in the vertically upward direction and the z - axis normal to the walls and the y -

axis is perpendicular to xz -plane [See Fig.1]. The walls and the fluid rotate in unison with uniform angular velocity Ω about z axis. Initially, at time $t \le 0$, both the walls and the fluid are assumed to be at the same temperature T_h and stationary. At time $t > 0$, the wall at $(z = 0)$ starts to move in its own plane with a velocity $U(t)$, and is heated with temperature $T_h + (T_0 - T_h)\frac{t}{t_0}$, T_0 being the temperature of the wall at $(z = 0)$ and t_0 a constant. The wall at $(z = h)$ is stationary and maintained at a constant temperature T_h. A uniform magnetic field of strength B_0 is imposed perpendicular to the walls. It is also assumed that the radiative heat flux in the x-direction is negligible in comparison with that in the z - direction. As the walls are infinitely long along x and y directions, the velocity and temperature fields are functions of z and t only. We assume that the magnetic Reynolds number for the flow is small so that the induced magnetic field can be neglected. This assumption is justified since the magnetic Reynolds number is generally very small for metallic liquid or partially ionized fluid.

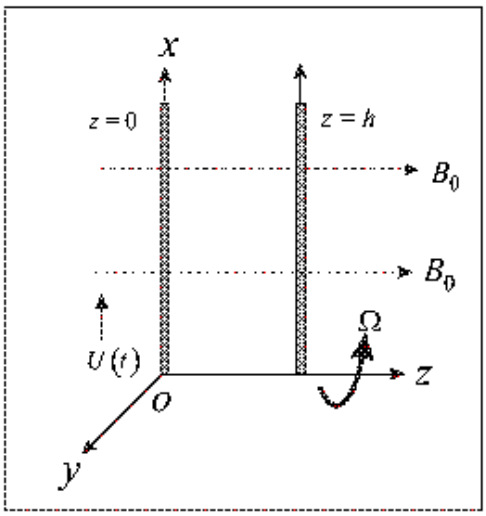

Fig.1: Geometry of the problem.

The generalized Ohm's law on taking Hall currents into account is [see Cowling [28]]

$$\vec{j} + \frac{\omega_e \tau_e}{B_0}\left(\vec{j} \times \vec{B}\right) = \sigma\left(\vec{E} + \vec{q} \times \vec{B}\right), \tag{1}$$

where $\vec{q}$, $\vec{B}$, $\vec{E}$, $\vec{j}$, σ, ω_e and τ_e are respectively the velocity vector, the magnetic field vector, the electric field vector, the current density vector, the electric conductivity, the cyclotron frequency and electron collision time. In writing the equation (1), the ion-slip and the thermoelectric effects as well as the electron pressure gradient are neglected.

The equation of continuity $\nabla \cdot \vec{q} = 0$ with no-slip condition at the plate gives $w = 0$ everywhere in the flow where $\vec{q} \equiv (u, v, w)$, u, v and w are respectively the velocity components along the coordinate axes. The solenoidal relation $\nabla \cdot \vec{B} = 0$ gives $B_z = \text{constant} = B_0$ everywhere in the flow where $\vec{B} \equiv (0, 0, B_z)$. The conservation of electric current $\nabla \cdot \vec{j} = 0$ yields $j_z =$ constant where $\vec{j} \equiv \left(j_x, j_y, j_z\right)$. This constant is zero since $j_z = 0$ at the plates which are electrically non-conducting. Hence, $j_z = 0$ everywhere in the flow. As the induced magnetic field is neglected, the Maxwell's equation $\nabla \times \vec{E} = -\frac{\partial \vec{B}}{\partial t}$ becomes $\nabla \times \vec{E} = 0$ which gives $\frac{\partial E_x}{\partial z} = 0$ and $\frac{\partial E_y}{\partial z} = 0$ where $\vec{E} \equiv \left(E_x, E_y, E_z\right)$. This implies that $E_x =$ constant and $E_y =$ constant everywhere in the flow.

In view of the above assumption, equation (1) yields

$$j_x + mj_y = \sigma(E_x + vB_0), \tag{2}$$

$$j_y - mj_x = \sigma(E_y - uB_0), \tag{3}$$

where $m = \omega_e \tau_e$ is the Hall parameter.

Further, we assume that $E = 0$ as there is no applied and polarization voltage exists. Hence, solving for j_x and j_y from equations (2) and (3) we have

$$j_x = \frac{\sigma B_0}{1+m^2}(v + mu), \tag{4}$$

$$j_y = \frac{\sigma B_0}{1+m^2}(mv - u), \tag{5}$$

where $m = \omega_e \tau_e$ is the Hall parameter.

Under the usual Boussinesq's approximation, on the use of (4) and (5), the fluid flow be governed by the following system of equations:

$$\frac{\partial u}{\partial t} - 2\Omega v = \nu \frac{\partial^2 u}{\partial z^2} + g\beta^*(T - T_h) - \frac{\sigma B_0^2}{\rho(1+m^2)}(u - mv), \tag{6}$$

$$\frac{\partial v}{\partial t} + 2\Omega u = \nu \frac{\partial^2 v}{\partial z^2} - \frac{\sigma B_0^2}{\rho(1+m^2)}(v + mu), \tag{7}$$

$$\rho c_p \frac{\partial T}{\partial t} = k \frac{\partial^2 T}{\partial z^2} - \frac{\partial q_r}{\partial z}, \tag{8}$$

where g is the acceleration due to gravity, T the fluid temperature, T_h the initial fluid temperature, β^* the coefficient of thermal expansion, ν the kinematic viscosity, ρ the fluid density, k the thermal conductivity, c_p the specific heat at constant pressure and q_r the radiative heat flux.

The initial and the boundary conditions for velocity and temperature distributions are

$u = 0 = v,\ T = T_h$ for $0 \le z \le h$ and $t \le 0$,

$$u = U(t),\ v = 0,\ T = T_h + (T_0 - T_h)\frac{t}{t_0} \text{ at } z = 0 \text{ for } t > 0, \tag{9}$$

$u = 0 = v,\ T = T_h$ at $z = h$ for $t > 0$.

It has been shown by Cogley et al.[29] that in the optically thin limit for a non-gray gas near equilibrium, the following relation holds

$$\frac{\partial q_r}{\partial y} = 4(T - T_h)\int_0^\infty K_{\lambda_h^*}\left(\frac{\partial e_{\lambda^* p}}{\partial T}\right)_h d\lambda^*, \tag{10}$$

where K_λ^* is the absorption coefficient, λ^* is the wave length, $e_{\lambda^* p}$ is the Planck's function and subscript $'h'$ indicates that all quantities have been evaluated at the temperature T_h which is the temperature of the wall at time $t \le 0$. Thus, our study is limited to small difference of wall temperature to the fluid temperature.

On the use of the equation (10), the equation (8) becomes

$$\rho c_p \frac{\partial T}{\partial t} = k\frac{\partial^2 T}{\partial y^2} - 4(T - T_h)I, \tag{11}$$

where

$$I = \int_0^\infty K_{\lambda_h^*}\left(\frac{\partial e_{\lambda^* p}}{\partial T}\right)_h d\lambda^*. \tag{12}$$

Introducing non-dimensional variables

$$\eta = \frac{z}{h},\ \tau = \frac{t}{t_0},\ (u_1, v_1) = \frac{(u,v)}{u_0},\ \theta = \frac{T - T_h}{T_0 - T_h},\ U(t) = u_0 f(\tau),\ t_0 = \frac{h^2}{\nu}, \tag{13}$$

equations (6), (7) and (11) become

$$\frac{\partial u_1}{\partial \tau} - 2K^2 v_1 = \frac{\partial^2 u_1}{\partial \eta^2} + Gr\theta - \frac{M^2}{1+m^2}(u_1 - mv_1), \tag{14}$$

$$\frac{\partial v_1}{\partial \tau} + 2K^2 u_1 = \frac{\partial^2 v_1}{\partial \eta^2} - \frac{M^2}{1+m^2}(v_1 + mu_1), \tag{15}$$

$$Pr\frac{\partial \theta}{\partial \tau} = \frac{\partial^2 \theta}{\partial \eta^2} - R\theta, \tag{16}$$

where $M^2 = \frac{\sigma B_0^2 h^2}{\rho\nu}$ is the magnetic parameter, $K^2 = \frac{\Omega h^2}{\nu}$ the rotation parameter, $R = \frac{4Ih^2}{k}$ the radiation parameter, $Gr = \frac{g\beta^*(T_0 - T_h)h^2}{\nu u_0}$ the Grashof number and $Pr = \frac{\rho\nu c_p}{k}$ the Prandtl number.

The corresponding initial and boundary conditions for u_1 and θ are

$$\begin{aligned} &u_1 = 0 = v_1, \theta = 0 \text{ for } 0 \le \eta \le 1 \text{ and } \tau \le 0,\\ &u_1 = f(\tau),\ v_1 = 0,\ \theta = \tau \text{ at } \eta = 0 \text{ for } \tau > 0,\\ &u_1 = 0 = v_1,\ \theta = 0 \text{ at } \eta = 1 \text{ for } \tau > 0. \end{aligned} \tag{17}$$

Combining equations (14) and (15), we get

$$\frac{\partial F}{\partial \tau} = \frac{\partial^2 F}{\partial \eta^2} + Gr\theta - \lambda^2 F, \tag{18}$$

where

$$F = u_1 + iv_1,\ \lambda^2 = \frac{M^2}{1+m^2} + i\left(2K^2 + \frac{mM^2}{1+m^2}\right) \text{ and } i = \sqrt{-1}. \tag{19}$$

The corresponding boundary conditions for F and θ are

$$\begin{aligned} &F = 0,\ \theta = 0 \text{ for } 0 \le \eta \le 1 \text{ and } \tau \le 0,\\ &F = f(\tau),\ \theta = \tau \text{ at } \eta = 0 \text{ for } \tau > 0,\\ &F = 0,\ \theta = 0 \text{ at } \eta = 1 \text{ for } \tau > 0. \end{aligned} \tag{20}$$

Taking the Laplace transformation, equations (18) and (16) become

$$s\bar{F} = \frac{d^2\bar{F}}{d\eta^2} + Gr\bar{\theta} - \lambda^2\bar{F}, \tag{21}$$

$$Prs\bar{\theta} = \frac{d^2\bar{\theta}}{d\eta^2} - R\bar{\theta}, \tag{22}$$

where

$$\bar{F}(\eta,s)=\int_0^\infty F(\eta,\tau)e^{-s\tau}\,d\tau \quad \text{and} \quad \bar{\theta}(\eta,s)=\int_0^\infty \theta(\eta,\tau)e^{-s\tau}\,d\tau. \tag{23}$$

The corresponding boundary conditions for $\bar{F}$ and $\bar{\theta}$ are

$$\bar{F}(0,s)=f(s),\ \bar{\theta}(0,s)=\frac{1}{s^2},$$
$$\bar{F}(1,s)=0,\ \bar{\theta}(1,s)=0, \tag{24}$$

where $f(s)$ is the Laplace transform of the function $f(\tau)$.

The solution of equations (21) and (22) subject to the boundary conditions (24) are given by

$$\bar{\theta}(\eta,s)=\begin{cases}\dfrac{1}{s^2}\dfrac{\sinh\sqrt{sPr+R}(1-\eta)}{\sinh\sqrt{sPr+R}} & \text{for } Pr\neq 1\\[2ex] \dfrac{1}{s^2}\dfrac{\sinh\sqrt{s+R}(1-\eta)}{\sinh\sqrt{s+R}} & \text{for } Pr=1,\end{cases} \tag{25}$$

$$\bar{F}(\eta,s)=\begin{cases} f(s)\dfrac{\sinh\sqrt{s+\lambda^2}(1-\eta)}{\sinh\sqrt{s+\lambda^2}} \\ \quad +\dfrac{Gr}{(Pr-1)(s+b)s^2}\left[\dfrac{\sinh\sqrt{s+\lambda^2}(1-\eta)}{\sinh\sqrt{s+\lambda^2}}-\dfrac{\sinh\sqrt{sPr+R}(1-\eta)}{\sinh\sqrt{sPr+R}}\right] & \text{for } Pr\neq 1\\[2ex] f(s)\dfrac{\sinh\sqrt{s+\lambda^2}(1-\eta)}{\sinh\sqrt{s+\lambda^2}} \\ \quad +\dfrac{Gr}{(R-\lambda^2)s^2}\left[\dfrac{\sinh\sqrt{s+\lambda^2}(1-\eta)}{\sinh\sqrt{s+\lambda^2}}-\dfrac{\sinh\sqrt{s+R}(1-\eta)}{\sinh\sqrt{s+R}}\right] & \text{for } Pr=1,\end{cases} \tag{26}$$

where $b=\dfrac{R-\lambda^2}{Pr-1}$.

Now, we consider the following cases:

(i) **When one of the walls $(\eta=0)$ starts to move impulsively:**

In this case $f(\tau)=1$, i.e. $f(s)=\dfrac{1}{s}$. The inverse Laplace transforms of equations (25) and (26) give the solution for the temperature and the velocity distributions respectively as

$$\theta(\eta,\tau)=\begin{cases}\tau\dfrac{\sinh\sqrt{R}(1-\eta)}{\sinh\sqrt{R}}+\dfrac{Pr}{2\sqrt{R}\sinh^2\sqrt{R}}\Big[(1-\eta)\cosh\sqrt{R}(1-\eta)\sinh\sqrt{R} \\ -\sinh\sqrt{R}(1-\eta)\cosh\sqrt{R}\Big]+2\sum_{n=0}^{\infty}n\pi\dfrac{e^{s_1\tau}}{s_1^2\,Pr}\sin n\pi\eta & \text{for } Pr\neq 1 \\ \tau\dfrac{\sinh\sqrt{R}(1-\eta)}{\sinh\sqrt{R}}+\dfrac{1}{2\sqrt{R}\sinh^2\sqrt{R}}\Big[(1-\eta)\cosh\sqrt{R}(1-\eta)\sinh\sqrt{R} \\ -\sinh\sqrt{R}(1-\eta)\cosh\sqrt{R}\Big]+2\sum_{n=0}^{\infty}n\pi\dfrac{e^{s_1\tau}}{s_1^2}\sin n\pi\eta & \text{for } Pr=1,\end{cases} \tag{27}$$

$$F(\eta,\tau)=\begin{cases}\dfrac{\sinh\lambda(1-\eta)}{\sinh\lambda}+2\sum_{n=0}^{\infty}n\pi\dfrac{e^{s_2\tau}}{s_2}\sin n\pi\eta+F_1(\eta,\tau,\lambda,Pr,\sqrt{R}) & \text{for } Pr\neq 1 \\ \dfrac{\sinh\lambda(1-\eta)}{\sinh\lambda}+2\sum_{n=0}^{\infty}n\pi\dfrac{e^{s_2\tau}}{s_2}\sin n\pi\eta+F_2(\eta,\tau,\lambda,\sqrt{R}) & \text{for } Pr=1,\end{cases} \tag{28}$$

where

$$F_1(\eta,\tau,\lambda,Pr,\sqrt{R})=\frac{Gr}{Pr-1}\Bigg[\frac{1}{b^2}(\tau b-1)\left\{\frac{\sinh\lambda(1-\eta)}{\sinh\lambda}-\frac{\sinh\sqrt{R}(1-\eta)}{\sinh\sqrt{R}}\right\}$$

$$+\frac{1}{2b\lambda\sinh^2\lambda}\{(1-\eta)\cosh\lambda(1-\eta)\sinh\lambda-\sinh\lambda(1-\eta)\cosh\lambda\}$$

$$-\frac{Pr}{2b\sqrt{R}\sinh^2\sqrt{R}}\{(1-\eta)\cosh\sqrt{R}(1-\eta)\sinh\sqrt{R}\ -\sinh\sqrt{R}(1-\eta)\cosh\sqrt{R}\}$$

$$+2\sum_{n=0}^{\infty}n\pi\left\{\frac{e^{s_2\tau}}{s_2^2(s_2+b)}-\frac{e^{s_1\tau}}{s_1^2(s_1+b)Pr}\right\}\sin n\pi\eta\Bigg],$$

$$F_2(\eta,\tau,\lambda,\sqrt{R})=\frac{Gr}{R-\lambda^2}\Bigg[\tau\left\{\frac{\sinh\lambda(1-\eta)}{\sinh\lambda}-\frac{\sinh\sqrt{R}(1-\eta)}{\sinh\sqrt{R}}\right\} \tag{29}$$

$$+\frac{1}{2\lambda\sinh^2\lambda}\{(1-\eta)\cosh\lambda(1-\eta)\sinh\lambda-\sinh\lambda(1-\eta)\cosh\lambda\}$$

$$-\frac{1}{2\sqrt{R}\sinh^2\sqrt{R}}\{(1-\eta)\cosh\sqrt{R}(1-\eta)\sinh\sqrt{R}\ -\sinh\sqrt{R}(1-\eta)\cosh\sqrt{R}\}$$

$$+2\sum_{n=0}^{\infty}n\pi\left\{\frac{e^{s_2\tau}}{s_2^2}-\frac{e^{s_1\tau}}{s_1^2}\right\}\sin n\pi\eta\Bigg],$$

$$s_1=-\frac{(n^2\pi^2+R)}{Pr},\quad s_2=-(n^2\pi^2+\lambda^2),$$

λ is given by (19). On separating into a real and imaginary parts one can easily obtain the velocity components u_1 and v_1 from equation (28).

For large time τ, equations (27) and (28) become

$$\theta(\eta,\tau)=\begin{cases}\tau\dfrac{\sinh\sqrt{R}(1-\eta)}{\sinh\sqrt{R}}+\dfrac{Pr}{2\sqrt{R}\sinh^2\sqrt{R}}\Big[(1-\eta)\cosh\sqrt{R}(1-\eta)\sinh\sqrt{R} & \\ -\sinh\sqrt{R}(1-\eta)\cosh\sqrt{R}\Big] & \text{for } Pr\neq 1 \\ \tau\dfrac{\sinh\sqrt{R}(1-\eta)}{\sinh\sqrt{R}}+\dfrac{1}{2\sqrt{R}\sinh^2\sqrt{R}}\Big[(1-\eta)\cosh\sqrt{R}(1-\eta)\sinh\sqrt{R} & \\ -\sinh\sqrt{R}(1-\eta)\cosh\sqrt{R}\Big] & \text{for } Pr=1,\end{cases} \tag{30}$$

$$F(\eta,\tau)=\begin{cases}\dfrac{\sinh\lambda(1-\eta)}{\sinh\lambda}+F_1(\eta,\tau,\lambda,Pr,\sqrt{R}) & \text{for } Pr\neq 1 \\ \dfrac{\sinh\lambda(1-\eta)}{\sinh\lambda}+F_2(\eta,\tau,\lambda,\sqrt{R}) & \text{for } Pr=1,\end{cases} \tag{31}$$

where

$$F_1(\eta,\tau,\lambda,Pr,\sqrt{R})=\frac{Gr}{Pr-1}\Bigg[\frac{1}{b^2}(\tau b-1)\Big\{\frac{\sinh\lambda(1-\eta)}{\sinh\lambda}-\frac{\sinh\sqrt{R}(1-\eta)}{\sinh\sqrt{R}}\Big\}$$

$$+\frac{1}{2b\lambda\sinh^2\lambda}\{(1-\eta)\cosh\lambda(1-\eta)\sinh\lambda-\sinh\lambda(1-\eta)\cosh\lambda\}$$

$$-\frac{Pr}{2b\sqrt{R}\sinh^2\sqrt{R}}\Big\{(1-\eta)\cosh\sqrt{R}(1-\eta)\sinh\sqrt{R}\ -\sinh\sqrt{R}(1-\eta)\cosh\sqrt{R}\Big\}\Bigg],$$

$$F_2(\eta,\tau,\lambda,\sqrt{R})=\frac{Gr}{R-\lambda^2}\Bigg[\tau\Big\{\frac{\sinh\lambda(1-\eta)}{\sinh\lambda}-\frac{\sinh\sqrt{R}(1-\eta)}{\sinh\sqrt{R}}\Big\} \tag{32}$$

$$+\frac{1}{2\lambda\sinh^2\lambda}\{(1-\eta)\cosh\lambda(1-\eta)\sinh\lambda-\sinh\lambda(1-\eta)\cosh\lambda\}$$

$$-\frac{1}{2\sqrt{R}\sinh^2\sqrt{R}}\Big\{(1-\eta)\cosh\sqrt{R}(1-\eta)\sinh\sqrt{R}\ -\sinh\sqrt{R}(1-\eta)\cosh\sqrt{R}\Big\}\Bigg],$$

and λ is given by (19).

(ii) When one of the wall $(\eta=0)$ starts to move accelerately:

In this case $f(\tau)=\tau$, i.e. $f(s)=\dfrac{1}{s^2}$. The inverse Laplace transforms of equations (25) and (26) yield

$$\theta(\eta,\tau)=\begin{cases}\tau\dfrac{\sinh\sqrt{R}(1-\eta)}{\sinh\sqrt{R}}+\dfrac{Pr}{2\sqrt{R}\sinh^2\sqrt{R}}\Big[(1-\eta)\cosh\sqrt{R}(1-\eta)\sinh\sqrt{R} & \\ -\sinh\sqrt{R}(1-\eta)\cosh\sqrt{R}\Big]+2\sum_{n=0}^{\infty}n\pi\dfrac{e^{s_1\tau}}{s_1^2\,Pr}\sin n\pi\eta & \text{for } Pr\neq 1 \\ \tau\dfrac{\sinh\sqrt{R}(1-\eta)}{\sinh\sqrt{R}}+\dfrac{1}{2\sqrt{R}\sinh^2\sqrt{R}}\Big[(1-\eta)\cosh\sqrt{R}(1-\eta)\sinh\sqrt{R} & \\ -\sinh\sqrt{R}(1-\eta)\cosh\sqrt{R}\Big]+2\sum_{n=0}^{\infty}n\pi\dfrac{e^{s_1\tau}}{s_1^2}\sin n\pi\eta & \text{for } Pr=1,\end{cases} \tag{33}$$

$$F(\eta,\tau)=\begin{cases}\tau\dfrac{\sinh\lambda(1-\eta)}{\sinh\lambda}+\dfrac{1}{2\lambda\sinh^2\lambda}\{(1-\eta)\cosh\lambda(1-\eta)\sinh\lambda \\ -\sinh\lambda(1-\eta)\cosh\lambda\} \\ +2\sum_{n=0}^{\infty}n\pi\dfrac{e^{s_2\tau}}{s_2^2}\sin n\pi\eta+F_1(\eta,\tau,\lambda,Pr,\sqrt{R}) & \text{for } Pr\neq 1 \\ \tau\dfrac{\sinh\lambda(1-\eta)}{\sinh\lambda}+\dfrac{1}{2\lambda\sinh^2\lambda}\{(1-\eta)\cosh\lambda(1-\eta)\sinh\lambda \\ -\sinh\lambda(1-\eta)\cosh\lambda\} \\ +2\sum_{n=0}^{\infty}n\pi\dfrac{e^{s_2\tau}}{s_2^2}\sin n\pi\eta+F_2(\eta,\tau,\lambda,\sqrt{R}) & \text{for } Pr=1,\end{cases} \tag{34}$$

where λ is given by (19), $F_1(\eta,\tau,\lambda,Pr,\sqrt{R})$, $F_2(\eta,\tau,\lambda,\sqrt{R})$, s_1 and s_2 are given by (29). On separating into a real and imaginary parts one can easily obtain the velocity components u_1 and v_1 from equation (34).

For large time τ, equations (33) and (34) become

$$\theta(\eta,\tau)=\begin{cases}\tau\dfrac{\sinh\sqrt{R}(1-\eta)}{\sinh\sqrt{R}}+\dfrac{Pr}{2\sqrt{R}\sinh^2\sqrt{R}}\Big[(1-\eta)\cosh\sqrt{R}(1-\eta)\sinh\sqrt{R} \\ -\sinh\sqrt{R}(1-\eta)\cosh\sqrt{R}\Big] & \text{for } Pr\neq 1 \\ \tau\dfrac{\sinh\sqrt{R}(1-\eta)}{\sinh\sqrt{R}}+\dfrac{1}{2\sqrt{R}\sinh^2\sqrt{R}}\Big[(1-\eta)\cosh\sqrt{R}(1-\eta)\sinh\sqrt{R} \\ -\sinh\sqrt{R}(1-\eta)\cosh\sqrt{R}\Big] & \text{for } Pr=1,\end{cases} \tag{35}$$

$$F(\eta,\tau)=\begin{cases}\tau\dfrac{\sinh\lambda(1-\eta)}{\sinh\lambda}+\dfrac{1}{2\lambda\sinh^2\lambda}\{(1-\eta)\cosh\lambda(1-\eta)\sinh\lambda \\ -\sinh\lambda(1-\eta)\cosh\lambda\} \\ +F_1(\eta,\tau,\lambda,Pr,\sqrt{R}) & \text{for } Pr\neq 1 \\ \tau\dfrac{\sinh\lambda(1-\eta)}{\sinh\lambda}+\dfrac{1}{2\lambda\sinh^2\lambda}\{(1-\eta)\cosh\lambda(1-\eta)\sinh\lambda \\ -\sinh\lambda(1-\eta)\cosh\lambda\} \\ +F_2(\eta,\tau,\lambda,\sqrt{R}) & \text{for } Pr=1,\end{cases} \tag{36}$$

where λ is given by (19), $F_1(\eta,\tau,\lambda,Pr,\sqrt{R})$ and $F_2(\eta,\tau,\lambda,\sqrt{R})$ are given by (32).

In the absence of Hall currents $(m=0)$, equations (28) and (34) are identical with the equations (23) and (29) of Sarkar et. al. [19].

RESULTS AND DISCUSSION

We have presented the non-dimensional velocity and temperature distributions for several values of magnetic parameter M^2, Rotation parameter K^2, Hall parameter m, radiation parameter R and time τ in Figs.2-14 for both the impulsive as well as the accelerated motion of one of the walls. It is seen from Fig.2 that the primary velocity u_1 decreases for both impulsive as well as accelerated motions of one of the walls with an increase in magnetic

parameter M^2. The presence of a magnetic field normal to the flow in an electrically conducting fluid introduces a Lorentz force which acts against the flow. This resistive force tends to slow down the flows and hence the fluid velocities decrease with an increase in magnetic parameter M^2. This trend is consistent with many classical studies on magneto-convection flow. Fig.3 reveals that the primary velocity u_1 decreases in the region $0 \le \eta < 0.43$ and then it increases for both the impulsive as well as the accelerated motions of one of the walls with an increase in rotation parameter K^2. The rotation parameter K^2 defines the relative magnitude of the Coriolis force and the viscous force in the regime, therefore it is clear that the high magnitude Coriolis forces are counter-productive for the primary velocity. It is seen from Fig.4 that the primary velocity u_1 decreases in the region $0 \le \eta < 0.23$ and $0 \le \eta < 0.27$ respectively and then it increases for both the impulsive as well as the accelerated motions of one of the walls with an increase in Hall parameter m. It is seen from Fig.5 that an increase in radiation parameter R leads to a decrease in primary velocity for both the impulsive and the accelerated motion of one of the walls. It indicates that radiation has a retarding influence on the primary velocity. It is revealed from Fig.6 that the primary velocity u_1 decreases for the impulsive motion whereas it increases in the region $0 \le \eta < 0.32$ and then decreases for the accelerated motion with an increase in time τ. It is noted from Figs. 2-6 that the primary velocity for the impulsive motion is greater than that of the accelerated motion near the wall $(\eta = 0)$. It is observed from Fig.7 and Fig.8 that the secondary velocity v_1 increases near the wall $(\eta = 0)$ while it decreases away from the wall $(\eta = 0)$ for both the impulsive and the accelerated motions of one of the walls with an increase in either magnetic parameter M^2 or rotation parameter K^2. It means that the magnetic field and rotation tend to enhance the secondary velocity in the vicinity of the wall $(\eta = 0)$ and to reduce it near the wall $(\eta = 1)$. It is illustrated from Fig.9 that the secondary velocity v_1 decreases near the wall $(\eta = 0)$ while it increases near the wall $(\eta = 1)$ for both the impulsive as well as the accelerated motions of one of the walls with an increase in Hall parameter m. It means that Hall currents have a tendency to reduce the secondary velocity in the vicinity of the wall $(\eta = 0)$ and to enhance it near the wall $(\eta = 1)$. Fig.10 reveals that the secondary velocity v_1 increases for both the impulsive and the accelerated motion of one of the walls with an increase in radiation parameter R. It is observed from Fig.11 that the secondary velocity v_1 decreases for the impulsive motion whereas it increases for the accelerated motion as time τ progresses. From Figs.7-11, it is interesting to note that the secondary velocity for the impulsive motion is greater than that of the accelerated motion of one of the walls. Further, it is seen from Figs.2-11 that the value of the fluid velocity components become negative at the middle region between two walls which indicates that there occurs a reverse flow at that region. Physically this is possible as the motion of the fluid is due to the motion of the wall in the upward direction against the gravitational field.

Effects of radiation parameter R, Prandtl number Pr and time τ on the temperature distribution have been shown in Figs.12-14. It is observed from Fig.12 that the fluid temperature $\theta(\eta, \tau)$ decreases with an increase in radiation parameter R. This result qualitatively agrees with expectations, since the effect of radiation decrease the rate of energy transport to the fluid, thereby decreasing the temperature of the fluid. Fig.13 shows that the fluid temperature $\theta(\eta, \tau)$ decreases with an increase in Prandtl number Pr. The Prandtl number Pr is the ratio of the viscosity to the thermal diffusivity. An increase in thermal diffusivity leads to a decrease in Prandtl number. Therefore, thermal diffusion has a tendency to reduce the fluid temperature. It is revealed from Fig.14 that an increase in time τ leads to rise in the fluid temperature distribution $\theta(\eta, \tau)$. It indicates that there is an enhancement in fluid temperature as time progresses.

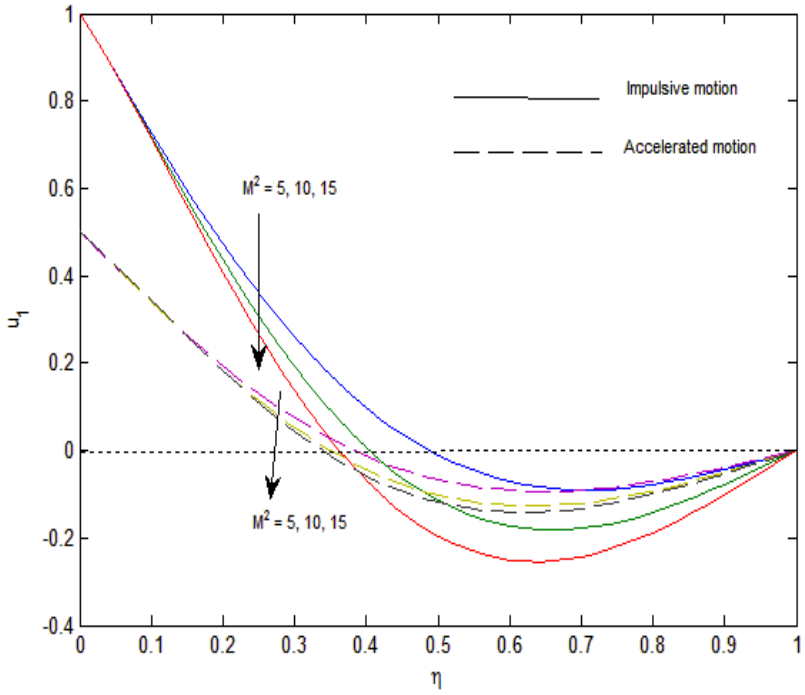

Fig.2: Primary velocity for M^2 **with** $R=3$, $K^2=5$, $Pr=0.03$, $Gr=5$, $m=0.5$ **and** $\tau=0.5$

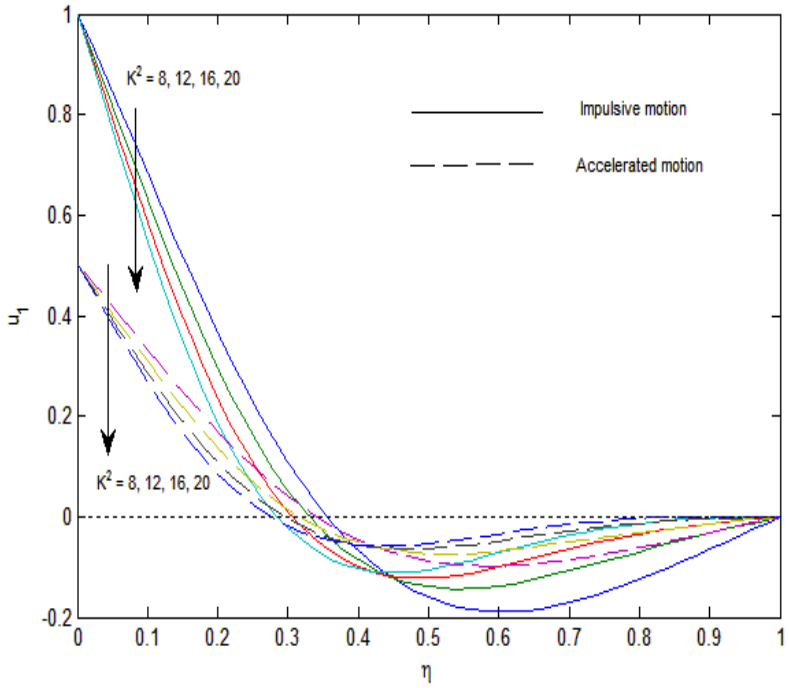

Fig.3: Primary velocity for K^2 **with** $R=1$, $M^2=15$, $Pr=0.03$, $Gr=5$, $m=0.5$ **and** $\tau=0.5$

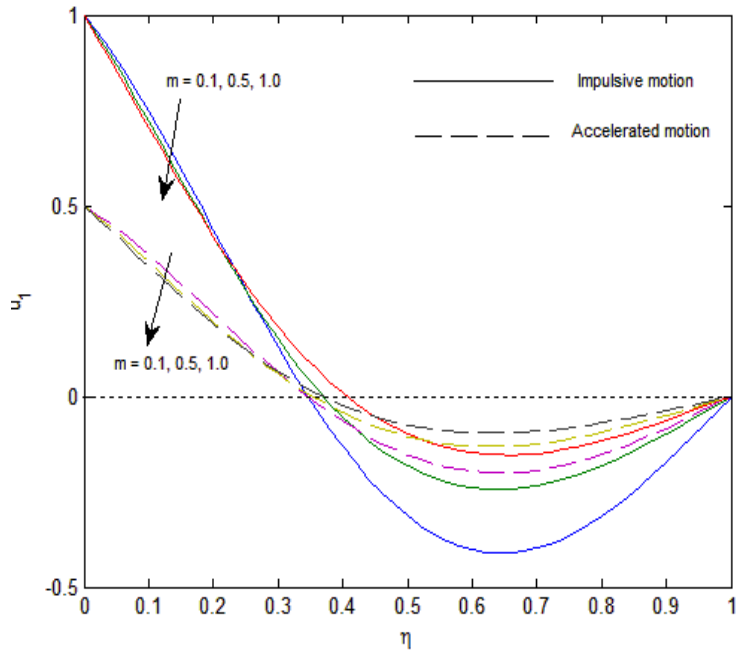

Fig.4: Primary velocity for m with $R=1$, $M^2=15$, $Pr=0.03$, $Gr=5$, $K^2=5$ and $\tau=0.5$

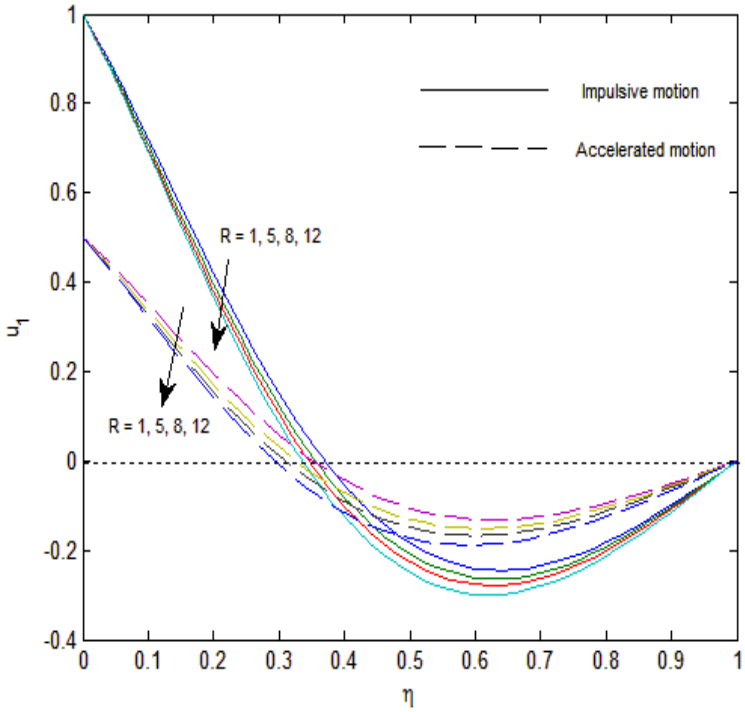

Fig.5: Primary velocity for R with $Gr=15$, $M^2=2$, $Pr=0.03$, $K^2=5$, $m=0.5$ and $\tau=0.5$

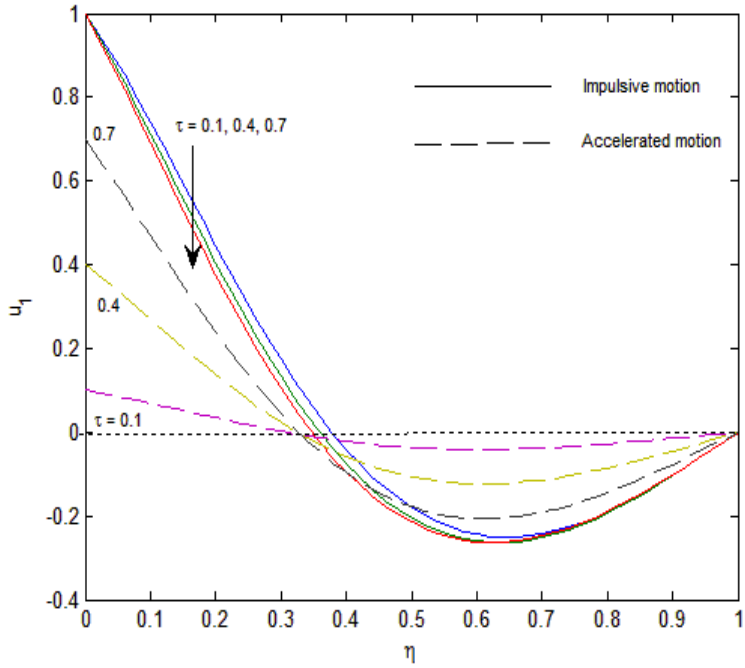

Fig.6: Primary velocity for τ with $R=1$, $M^2=15$, $Gr=5$, $K^2=5$, $m=0.5$ and $Pr=0.03$

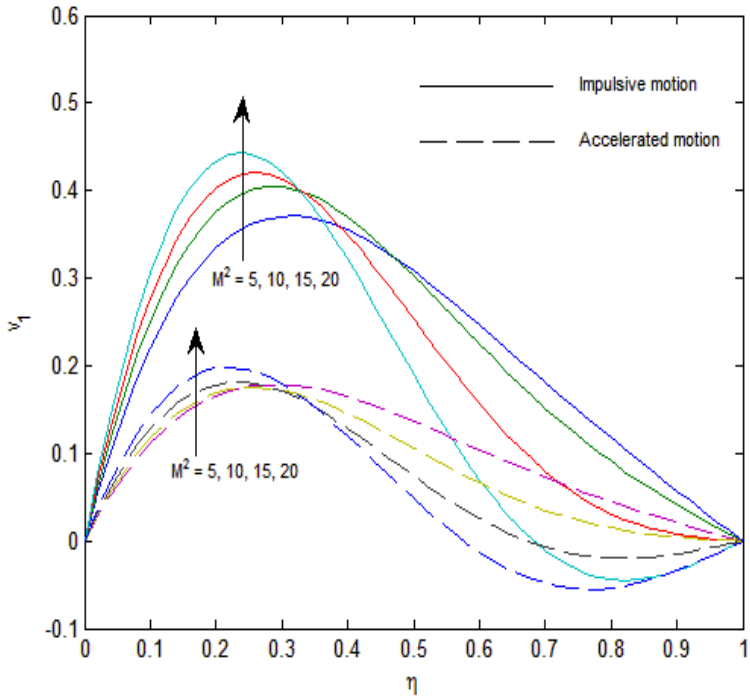

Fig.7: Secondary velocity for M^2 with $R=3$, $K^2=5$, $Pr=0.03$, $Gr=5$, $m=0.5$ and $\tau=0.5$

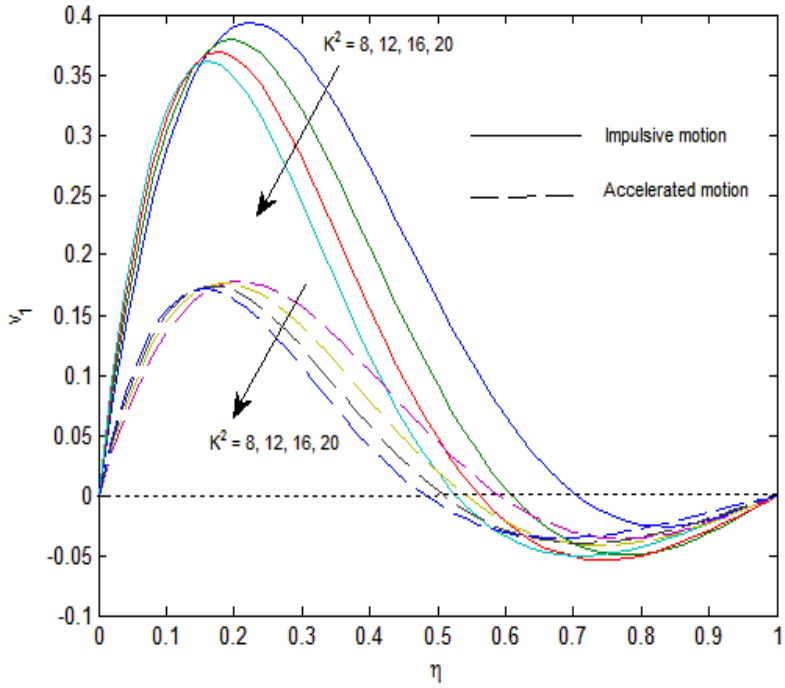

Fig.8: Secondary velocity for K^2 with $R=1$, $M^2=15$, $Pr=0.03$, $Gr=5$, $m=0.5$ and $\tau=0.5$

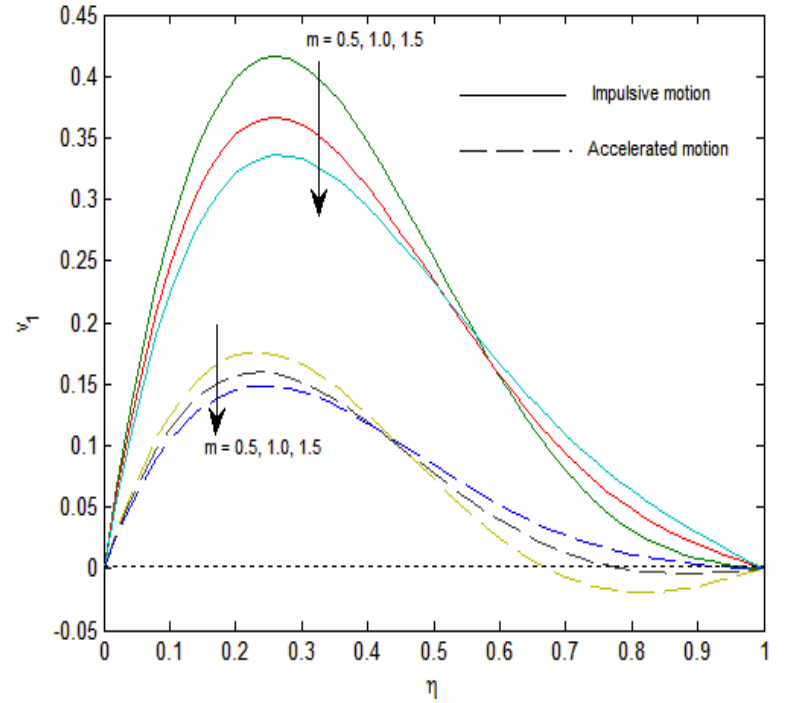

Fig.9: Secondary velocity for m with $R=1$, $M^2=15$, $Pr=0.03$, $Gr=5$, $K^2=5$ and $\tau=0.5$

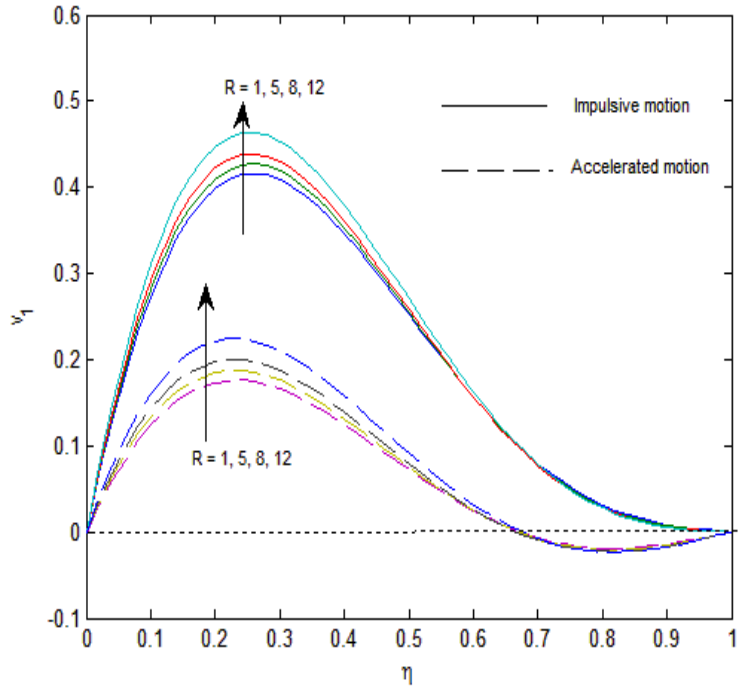

Fig.10: Secondary velocity for R with $Gr = 15$, $M^2 = 2$, $Pr = 0.03$, $K^2 = 5$, $m = 0.5$ and $\tau = 0.5$

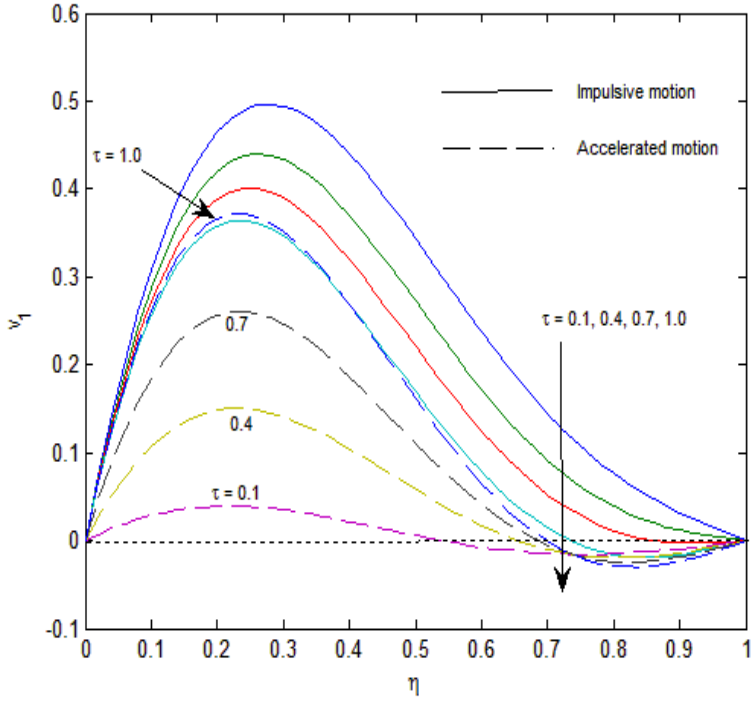

Fig.11: Secondary velocity for τ with $R = 1$, $M^2 = 15$, $Gr = 5$, $K^2 = 5$, $m = 0.5$ and $Pr = 0.03$

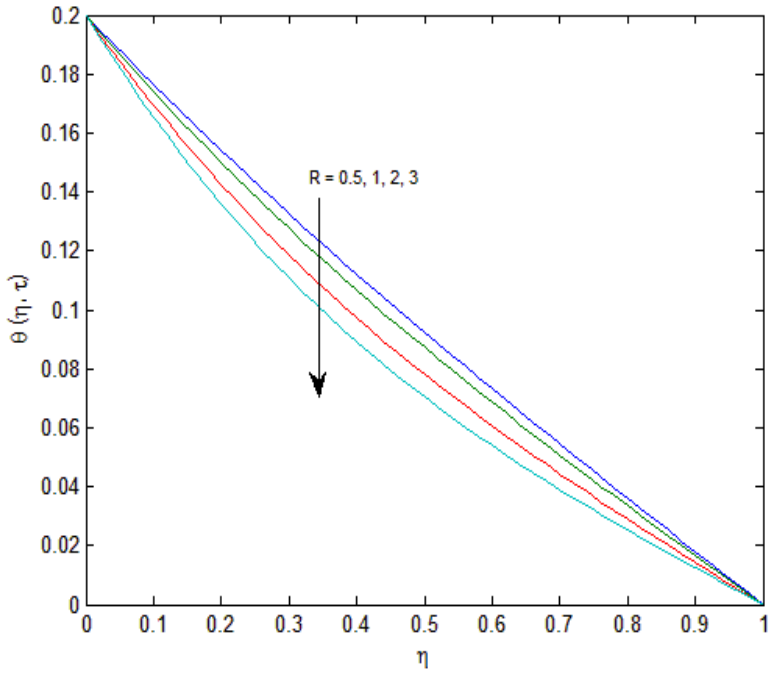

Fig.12: Temperature profiles for R with $\tau = 0.2$ and $Pr = 0.03$

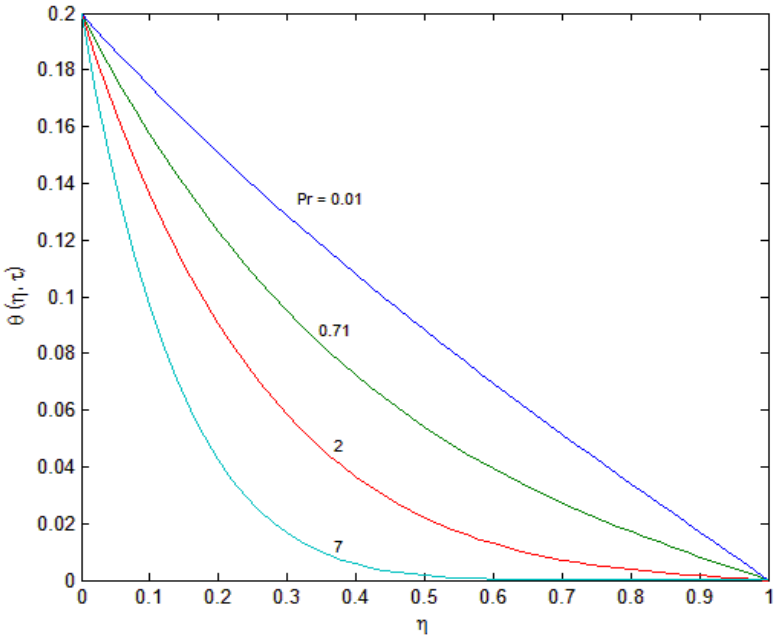

Fig.13: Temperature profiles for Pr with $\tau = 0.2$ and $R = 1$

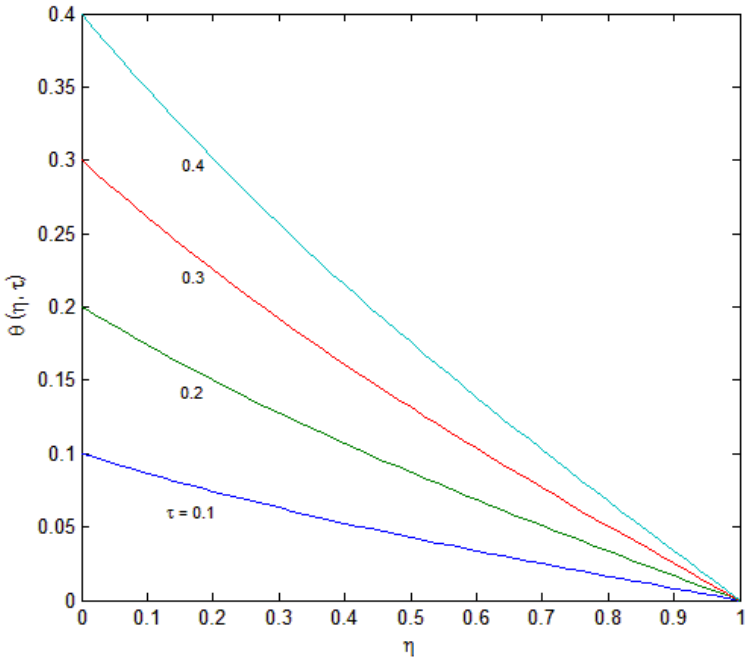

Fig.14: Temperature profiles for τ with $R=1$ and $Pr=0.03$

For impulsive motion, the non-dimensional shear stresses at the walls $(\eta=0)$ and $(\eta=1)$ are respectively obtained as follows:

$$\tau_{x_0}+i\tau_{y_0}=\left(\frac{\partial F}{\partial \eta}\right)_{\eta=0}$$

$$=\begin{cases}-\lambda\coth\lambda+2\sum_{n=0}^{\infty}n^2\pi^2\dfrac{e^{s_2\tau}}{s_2}+G_1(0,\tau,\lambda,Pr,\sqrt{R}) & \text{for } Pr\neq 1\\[2ex] -\lambda\coth\lambda+2\sum_{n=0}^{\infty}n^2\pi^2\dfrac{e^{s_2\tau}}{s_2}+G_2(0,\tau,\lambda,\sqrt{R}) & \text{for } Pr=1,\end{cases} \tag{37}$$

$$\tau_{x_1}+i\tau_{y_1}=\left(\frac{\partial F}{\partial \eta}\right)_{\eta=1}$$

$$=\begin{cases}-\lambda\operatorname{cosech}\lambda+2\sum_{n=0}^{\infty}n^2\pi^2(-1)^n\dfrac{e^{s_2\tau}}{s_2}+G_1(1,\tau,\lambda,Pr,\sqrt{R}) & \text{for } Pr\neq 1\\[2ex] -\lambda\operatorname{cosech}\lambda+2\sum_{n=0}^{\infty}n^2\pi^2(-1)^n\dfrac{e^{s_2\tau}}{s_2}+G_2(1,\tau,\lambda,\sqrt{R}) & \text{for } Pr=1,\end{cases} \tag{38}$$

where

$$G_1(0,\tau,\lambda,Pr,\sqrt{R})=\frac{Gr}{Pr-1}\left[\frac{1}{b^2}(\tau b-1)\left(\sqrt{R}\coth\sqrt{R}-\lambda\coth\lambda\right)+\frac{1}{2b\lambda\sinh^2\lambda}\left(\lambda-\cosh\lambda\sinh\lambda\right)\right.$$

$$\left.-\frac{Pr}{2b\sqrt{R}\sinh^2\sqrt{R}}\left(\sqrt{R}-\cosh\sqrt{R}\sinh\sqrt{R}\right)+2\sum_{n=0}^{\infty}n^2\pi^2\left\{\frac{e^{s_2\tau}}{s_2^{\,2}(s_2+b)}-\frac{e^{s_1\tau}}{s_1^{\,2}(s_1+b)Pr}\right\}\right],$$

$$G_1(1,\tau,\lambda,Pr,\sqrt{R}) = \frac{Gr}{Pr-1}\left[\frac{1}{b^2}(\tau b-1)\left(\sqrt{R}\,\text{cosech}\,\sqrt{R}-\lambda\,\text{cosech}\,\lambda\right)+\frac{1}{2b\lambda\sinh^2\lambda}(\lambda\cosh\lambda-\sinh\lambda)\right.$$

$$\left.-\frac{Pr}{2b\sqrt{R}\sinh^2\sqrt{R}}\left(\sqrt{R}\cosh\sqrt{R}-\sinh\sqrt{R}\right)+2\sum_{n=0}^{\infty}n^2\pi^2(-1)^n\left\{\frac{e^{s_2\tau}}{s_2^{\,2}(s_2+b)}-\frac{e^{s_1\tau}}{s_1^{\,2}(s_1+b)Pr}\right\}\right], \tag{39}$$

$$G_2(0,\tau,\lambda,\sqrt{R}) = \frac{Gr}{R-\lambda^2}\left[\tau\left(\sqrt{R}\coth\sqrt{R}-\lambda\coth\lambda\right)+\frac{1}{2\lambda\sinh^2\lambda}(\lambda-\cosh\lambda\sinh\lambda)\right.$$

$$\left.-\frac{1}{2\sqrt{R}\sinh^2\sqrt{R}}\left(\sqrt{R}-\cosh\sqrt{R}\sinh\sqrt{R}\right)+2\sum_{n=0}^{\infty}n^2\pi^2\left(\frac{e^{s_2\tau}}{s_2^{\,2}}-\frac{e^{s_1\tau}}{s_1^{\,2}}\right)\right],$$

$$G_2(1,\tau,\lambda,\sqrt{R}) = \frac{Gr}{R-\lambda^2}\left[\tau\left(\sqrt{R}\,\text{cosech}\,\sqrt{R}-\lambda\,\text{cosech}\,\lambda\right)+\frac{1}{2\lambda\sinh^2\lambda}(\lambda\cosh\lambda-\sinh\lambda)\right.$$

$$\left.-\frac{1}{2\sqrt{R}\sinh^2\sqrt{R}}\left(\sqrt{R}\cosh\sqrt{R}-\sinh\sqrt{R}\right)+2\sum_{n=0}^{\infty}n^2\pi^2(-1)^n\left(\frac{e^{s_2\tau}}{s_2^{\,2}}-\frac{e^{s_1\tau}}{s_1^{\,2}}\right)\right],$$

λ is given by (19), s_1 and s_2 are given by (29).

For accelerated motion, the non-dimensional shear stresses at the walls $(\eta=0)$ and $(\eta=1)$ are respectively obtained as follows:

$$\tau_{x_0}+i\tau_{y_0} = \left(\frac{\partial F}{\partial\eta}\right)_{\eta=0}$$

$$= \begin{cases} -\tau\lambda\coth\lambda+\dfrac{1}{2\lambda\sinh^2\lambda}(\lambda-\cosh\lambda\sinh\lambda) \\ 2\displaystyle\sum_{n=0}^{\infty}n^2\pi^2\frac{e^{s_2\tau}}{s_2^{\,2}}+G_1(0,\tau,\lambda,Pr,\sqrt{R}) \qquad \text{for } Pr\neq 1 \\ \\ -\tau\lambda\coth\lambda+\dfrac{1}{2\lambda\sinh^2\lambda}(\lambda-\cosh\lambda\sinh\lambda) \\ 2\displaystyle\sum_{n=0}^{\infty}n^2\pi^2\frac{e^{s_2\tau}}{s_2^{\,2}}+G_2(0,\tau,\lambda,\sqrt{R}) \qquad \text{for } Pr=1, \end{cases} \tag{40}$$

$$\tau_{x_1}+i\tau_{y_1} = \left(\frac{\partial F}{\partial\eta}\right)_{\eta=1}$$

$$= \begin{cases} -\tau\lambda\,\text{cosech}\,\lambda+\dfrac{1}{2\lambda\sinh^2\lambda}(\lambda\cosh\lambda-\sinh\lambda) \\ +2\displaystyle\sum_{n=0}^{\infty}n^2\pi^2(-1)^n\frac{e^{s_2\tau}}{s_2^{\,2}}+G_1(1,\tau,\lambda,Pr,\sqrt{R}) \qquad \text{for } Pr\neq 1 \\ \\ -\tau\lambda\,\text{cosech}\,\lambda+\dfrac{1}{2\lambda\sinh^2\lambda}(\lambda\cosh\lambda-\sinh\lambda) \\ +2\displaystyle\sum_{n=0}^{\infty}n^2\pi^2(-1)^n\frac{e^{s_2\tau}}{s_2^{\,2}}+G_2(1,\tau,\lambda,\sqrt{R}) \qquad \text{for } Pr=1, \end{cases} \tag{41}$$

where λ is given by (19), $G_1(0,\tau,\lambda,Pr,\sqrt{R})$, $G_1(1,\tau,\lambda,Pr,\sqrt{R})$, $G_2(0,\tau,\lambda,\sqrt{R})$ and $G_2(1,\tau,\lambda,\sqrt{R})$ are given by (39).

Numerical results of the non-dimensional shear stresses at the wall $(\eta = 0)$ are presented in Figs.15-18 against Hall parameter m for several values of rotation parameter K^2 and radiation parameter R when $M^2 = 10$, $\tau = 0.2$, $Gr = 5$ and $Pr = 0.03$. Figs.15 and 16 show that the absolute value of the shear stress τ_{x_0} at the wall $(\eta = 0)$ due to the primary flow increases with an increase in either rotation parameter K^2 or radiation parameter R or Hall parameter m for both the impulsive as well as the accelerated motion of one of the walls. It is observed from Figs.17 and 18 that the shear stress τ_{y_0} at the wall $(\eta = 0)$ due to the secondary flow increases with an increase in either rotation parameter K^2 or radiation parameter R whereas it decreases with an increase in Hall parameter m for both the impulsive and the accelerated motion. Further, it is observed from Figs.15-18 that the shear stresses at the wall $(\eta = 0)$ due to the primary and the secondary flow for the impulsive start is greater than that of the accelerated start one of the walls.

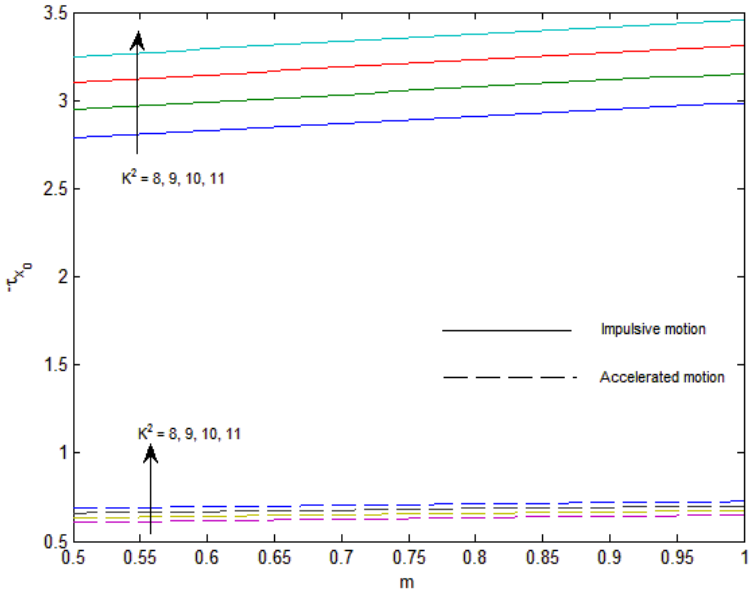

Fig.15: Shear stress τ_{x_0} due to primary flow for K^2 when $R = 1$

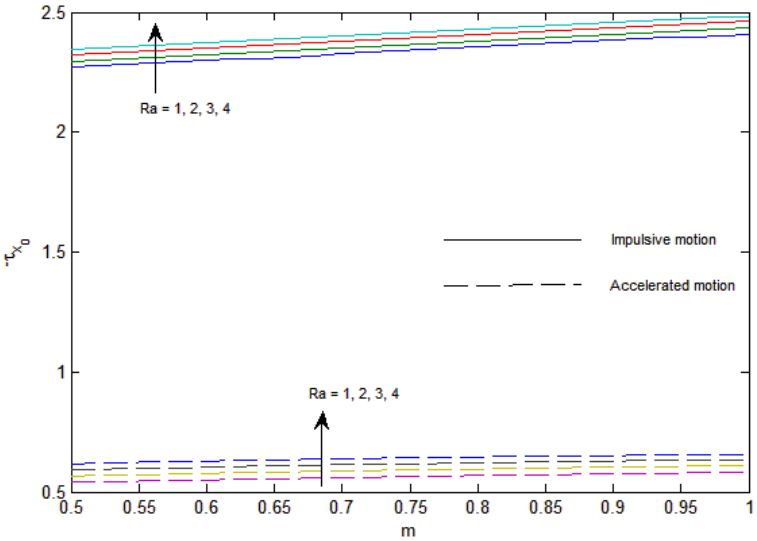

Fig.16: Shear stress τ_{x_0} due to primary flow for R when $K^2 = 5$

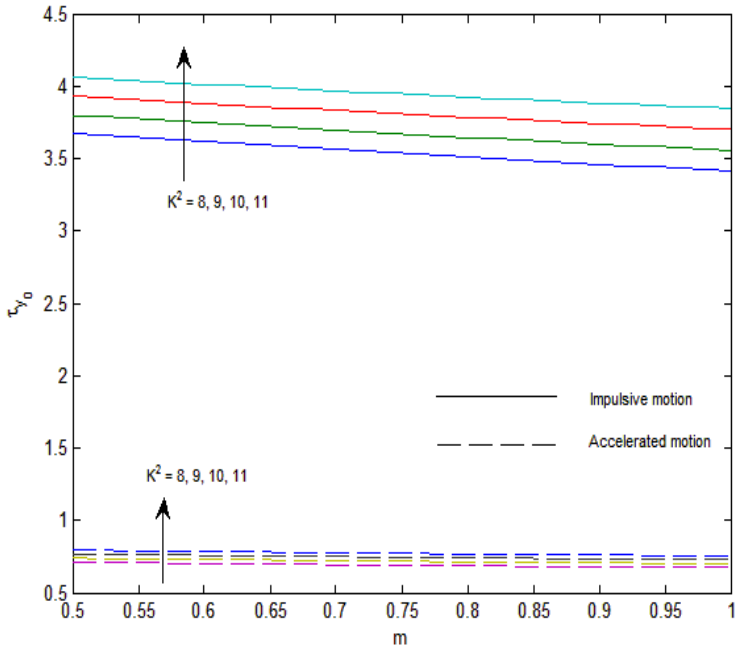

Fig.17: Shear stress τ_{y_0} due to secondary flow for K^2 when $R=1$

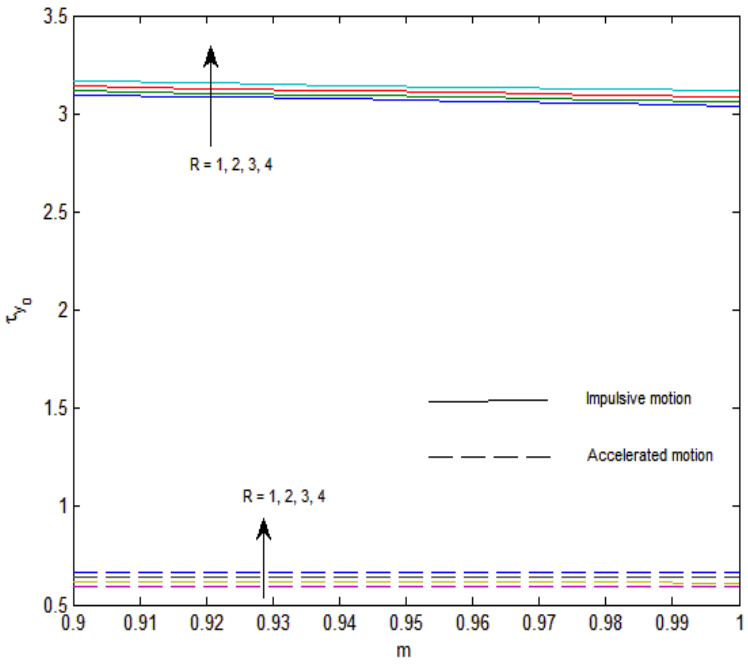

Fig.18: Shear stress τ_{y_0} due to secondary flow for R when $K^2=5$

The rate of heat transfer $\theta'(0,\tau)$ $\left(=\left.\frac{\partial\theta}{\partial\eta}\right|_{\eta=0}\right)$ at the wall $(\eta=0)$ and $\theta'(1,\tau)$ $\left(=\left.\frac{\partial\theta}{\partial\eta}\right|_{\eta=1}\right)$ at the wall $(\eta=1)$ are respectively given by

$$\theta'(0,\tau)=\begin{cases}-\tau\sqrt{R}\coth\sqrt{R}+\dfrac{Pr}{2\sqrt{R}\sinh^2\sqrt{R}}\left[\sqrt{R}-\cosh\sqrt{R}\sinh\sqrt{R}\right] & \\ +2\sum_{n=0}^{\infty}n^2\pi^2\dfrac{e^{s_1\tau}}{s_1^{\,2}Pr} & \text{for } Pr\neq 1\\ -\tau\sqrt{R}\coth\sqrt{R}+\dfrac{1}{2\sqrt{R}\sinh^2\sqrt{R}}\left[\sqrt{R}-\cosh\sqrt{R}\sinh\sqrt{R}\right] & \\ +2\sum_{n=0}^{\infty}n^2\pi^2\dfrac{e^{s_1\tau}}{s_1^{\,2}} & \text{for } Pr=1,\end{cases} \tag{42}$$

$$\theta'(1,\tau)=\begin{cases}-\tau\sqrt{R}\,\mathrm{cosech}\sqrt{R}+\dfrac{Pr}{2\sqrt{R}\sinh^2\sqrt{R}}\left[\sqrt{R}\cosh\sqrt{R}-\sinh\sqrt{R}\right] & \\ +2\sum_{n=0}^{\infty}n^2\pi^2(-1)^n\dfrac{e^{s_1\tau}}{s_1^{\,2}Pr} & \text{for } Pr\neq 1\\ -\tau\sqrt{R}\,\mathrm{cosech}\sqrt{R}+\dfrac{1}{2\sqrt{R}\sinh^2\sqrt{R}}\left[\sqrt{R}\cosh\sqrt{R}-\sinh\sqrt{R}\right] & \\ +2\sum_{n=0}^{\infty}n^2\pi^2(-1)^n\dfrac{e^{s_1\tau}}{s_1^{\,2}} & \text{for } Pr=1,\end{cases} \tag{43}$$

where s_1 is given by (29).

Numerical results of the rate of heat transfer $-\theta'(0,\tau)$ at the wall $(\eta=0)$ and $-\theta'(1,\tau)$ at the wall $(\eta=1)$ against the radiation parameter R are presented in the Table 1 and 2 for several values of Prandtl number Pr and time τ. Table 1 shows that the rate of heat transfer $-\theta'(0,\tau)$ increases whereas $-\theta'(1,\tau)$ decreases with an increase in Prandtl number Pr. It is observed from Table 2 that the rates of heat transfer $-\theta'(0,\tau)$ and $-\theta'(1,\tau)$ increase with an increase in time τ. Further, it is seen from Table 1 and 2 that the rate of heat transfer $-\theta'(0,\tau)$ increases whereas the rate of heat transfer $-\theta'(1,\tau)$ decreases with an increase in radiation parameter R.

Table 1. Rate of heat transfer at the wall $(\eta=0)$ and at the wall $(\eta=1)$

	$-\theta'(0,\tau)$				$-\theta'(1,\tau)$			
$R\setminus Pr$	0.01	0.71	1	2	0.01	0.71	1	2
0.5	0.23540	0.44719	0.52178	0.72549	0.18277	0.08573	0.05865	0.01529
1.0	0.26555	0.46614	0.53808	0.73721	0.16885	0.08117	0.05599	0.01483
1.5	0.29403	0.48461	0.55407	0.74881	0.15635	0.07690	0.05346	0.01438
2.0	0.32102	0.50262	0.56976	0.76030	0.14509	0.07290	0.05106	0.01394

Table 2. Rate of heat transfer at the wall $(\eta=0)$ and at the wall $(\eta=1)$

	$-\theta'(0,\tau)$				$-\theta'(1,\tau)$			
$R\setminus \tau$	0.1	0.2	0.3	0.4	0.1	0.2	0.3	0.4
0.5	0.12551	0.24165	0.35779	0.47392	0.08767	0.17980	0.27193	0.36405
1.0	0.14014	0.27144	0.40275	0.53405	0.08110	0.16619	0.25128	0.33637
1.5	0.15398	0.29960	0.44522	0.59084	0.07518	0.15396	0.23273	0.31151
2.0	0.16712	0.32631	0.48550	0.64469	0.06984	0.14292	0.21601	0.28909

CONCLUSION

The radiation effects on MHD free convective Couette flow in a rotating system confined between two infinitely long vertical walls with variable temperature have been studied on taking Hall currents into account. Magnetic field

and radiation have a retarding influence on the primary velocity. On the other hand, magnetic field has an accelerating influence near the moving wall and a retarding influence away from the moving wall whereas radiation has an accelerating influence on the secondary velocity for both the impulsive as well as the accelerated motion of one of the walls. Hall currents and rotation have grate influence on the velocity field. It is noted that the velocity for the impulsive motion is greater than that of the accelerated motion near the wall $(\eta = 0)$. An increase in either radiation parameter R or Prandtl number Pr leads to fall in the fluid temperature θ. There is an enhancement in fluid temperature as time progresses. Both the rotation and radiation enhance the absolute value of the shear stresses τ_{x_0} and τ_{y_0} at the wall $(\eta = 0)$ for both the impulsive as well as the accelerated motion. Further, the rate of heat transfer $-\theta'(0,\tau)$ at the wall $(\eta = 0)$ increases whereas the rate of heat transfer $-\theta'(1,\tau)$ at the wall $(\eta = 1)$ decreases with an increase in radiation parameter R.

REFERENCES

[1] A.K. Singh, *Defense Science Journal*, **1988**, 38(1), 35-41.
[2] A.K. Singh, T. Paul, *Int. J. Appl. Mech. Eng.*, **2006**, 11(1), 143-154.
[3] B.K. Jha, A.K. Singh, H.S. Takhar, *Int. J. Appl. Mech. Eng.*, **2003**, 8(3), 497-502.
[4] H.M. Joshi, *Int. Comm. in Heat and Mass Transfer*, **1988**, 15, 227-238.
[5] O. Miyatake and T. Fujii, *Heat Transfer Japan Res.*, **1972**, 1, 30-38.
[6] H. Tanaka, O. Miyatake, T. Fujii, M. Fujii, *Heat Transfer Japan Res.*, **1973**, 2, 25-33.
[7] H.S. Takhar and P.C. Ram, *Astrophysics and Space Science*, **1991**, 183, 193-198.
[8] A.K. Singh, H.R. Gholami and V.M. Soundalgekar, *Heat and Mass Transfer*, **1996**, 31, 329-331.
[9] B.K. Jha, *Heat and Mass Transfer*, **2001**, 37, 329-331.
[10] T. Grosan and I. Pop , *Technische Mechanik*, **2007**, 27(1), 37-47.
[11] B. K. Jha and A.O. Ajibade, *Int. J. Energy and Tech.*, **2010**, 2(12), 1–9.
[12] Al-Amri, G. Fahad , El-Shaarawi and Maged AI, *Int. J. Numer. Meth. Heat & Fluid Flow*, **2010**, 20(2), 218 - 239.
[13] M. Narahari, *WSEAS Transactions on Heat and Mass Transfer*, **2010**, 5(1), 21-30.
[14] U.S. Rajput and P.K. Sahu , *Int. Journal of Math. Analysis*, **2011**, 5(34), 1665 - 6671.
[15] U.S. Rajput and S. Kumar , *Int. J. Math. Analysis*, 5(24), **2011**, 1155 - 1163.
[16] S. S. Saxena and G.K. Dubey, *Adva. Appl. Sci. Res.*, **2011**, 2 (4), 259-278.
[17] V. Sri Hari Babu and G.V. Ramana Reddy, *Adva. Appl. Sci. Res.*, **2011**, 2 (4), 138-146.
[18] S. S. Saxena and G.K. Dubey, *Adva. Appl. Sci. Res.*, **2011**, 2 (5), 115-129.
[19] G. Sudershan Reddy, G.V. Ramana Reddy and K. Jayarami Reddy, *Adva. Appl. Sci. Res.*, **2012**, 3(3), 1603-1610.
[20] S. P. Anjali Devi and A. David Maxim Gururaj, *Adva. Appl. Sci. Res.*, **2012**, 3 (1), 319 - 334.
[21] K. Jayarami Reddy, K. Sunitha and M. Jayabharath Reddy, *Adva. Appl. Sci. Res.*, **2012**, 3(3), 1231-1238.
[22] K. D. Singh and R. Pathak, *Int. J. Pure and Appl. Physics.*, **2012**, 50, 77-85.
[23] S. Das, B.C. Sarkar and R.N. Jana, *Open J. Fluid Dynamics*, **2012**, 2, 14-27.
[24] C. Mandal, S. Das and R.N. Jana , *Int. J. Appl. Inf. Systems*, **2012**, 2(2), 49-56.
[25] B. C. Sarkar, S. Das and R.N. Jana, *Int. J. Eng. Res. and Appl.*, **2012**, 2(4), 2346-2359.
[26] B. C. Sarkar, S. Das and R.N. Jana, *Adva. Appl. Sci. Res.*, **2012**, 3 (5), 3291-3310.
[27] B. C. Sarkar, S. Das and R.N. Jana, *Adva. Appl. Sci. Res.*, **2012**, 3 (5), 3311-3325.
[28] T. G. Cowling, Magnetohydrodynamics, *New York, Interscience*, **1957**, 101.
[29] A. C. Cogley, W.C. Vincentine and S.E. Gilles, *AIAA Journal*, **1968**, 6, 551-555.